Available online at www.sciencedirect.com

ScienceDirect

journal homepage: www.elsevier.com/locate/he

Numerical investigation of premixed hydrogen/air combustion at lean to ultra-lean conditions and catalytic approach to enhance stability

Md Nur Alam Mondal [a], *Nader Karimi* [a,c], *S. David Jackson* [b], *Manosh C. Paul* [a,*]

[a] *James Watt School of Engineering, University of Glasgow, Glasgow, G12 8QQ, United Kingdom*
[b] *School of Chemistry, University of Glasgow, Glasgow, G12 8QQ, United Kingdom*
[c] *School of Engineering and Materials Science, Queen Mary University of London, London, E14NS, United Kingdom*

HIGHLIGHTS

- Premixed hydrogen/air combustion at lean to ultra-lean conditions.
- A stability map is presented for non-catalytic combustion.
- Catalyst enhances flame stability and provides complete hydrogen combustion.
- Radiation significantly affects combustion kinetics and flame temperature.
- NO_x emission at lean to ultra-lean conditions investigated.

GRAPHICAL ABSTRACT

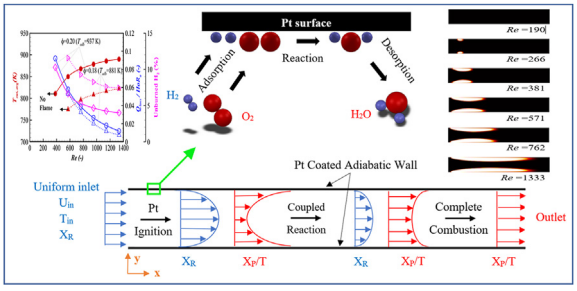

ARTICLE INFO

Article history:
Received 16 November 2022
Received in revised form
19 January 2023
Accepted 24 January 2023
Available online 14 February 2023

Keywords:
Hydrogen
Premixed
Lean
Catalytic combustion
Platinum catalyst
NO_x emission

ABSTRACT

Premixed combustion of hydrogen/air over a platinum (Pt) catalyst is numerically investigated in a planar channel burner with the aim of stabilising the flame at lean to ultra-lean conditions. A steady laminar species transport model is examined in conjunction with elementary heterogeneous and homogeneous chemical reaction schemes and validated against experimental results. A stability map is obtained in a non-catalytic burner for the equivalence ratios (φ) of 0.15–0.20, which serves as the basis for the catalytic flame analysis. Over the Reynolds numbers (Re) investigated in the non-catalytic burner, no flame is observed for $\varphi \leq 0.16$, and flame extinction occurs at $Re < 571$ and $Re < 381$ for $\varphi = 0.18$ and 0.20, respectively. Moreover, a significant amount of unburned H_2 exits the burner in all cases. With the Pt catalyst coated on the walls, complete H_2 combustion is attained for $0.10 \leq \varphi \leq 0.20$ where the contribution of gas phase (homogeneous) reaction increases with Re. Furthermore, radiation on the wall and at the inlet affects the combustion kinetics and flame temperature. Finally, NO_x emission is investigated under the same conditions and found to increase with equivalence ratio but has a negligible effect with the inflow Reynolds number.

* *Corresponding author.*
E-mail address: Manosh.Paul@glasgow.ac.uk (M.C. Paul).
https://doi.org/10.1016/j.ijhydene.2023.01.298

Nomenclature

D_m	mass diffusivity (m^2/s)
e	total energy (J/kg)
G	radiation intensity (W/m^2)
h_i	enthalpy (J/kg) of species (i)
HoR	heat of reaction (W)
h	burner height (m)
J_i	diffusion flux (kg/m^2s) of species (i)
k_c	mass transfer coefficient (–)
L	burner wall (m)
Le	Lewis number (–)
m	total number of surface species (–)
n	total number of gas species (–)
p	pressure (Pa)
Q_{loss}	net heat loss (W)
Q_{rad}	radiation heat (W)
q_{rad}	radiation heat flux (W/m^2)
R	reaction rate (kg/m^3s)
Re	Reynolds number (–)
s	molar production rate (mol/m^2s)
Sh	Sherwood number (–)
T	temperature (K)
U_{in}	inlet velocity (m/s)
X	mole fraction (–)
Y	mass fraction (–)
x	streamwise coordinate (m)
y	transverse coordinate (m)

Greek symbols

ρ	density (kg/m^3)
μ	dynamic viscosity (kg/ms)
φ	equivalence ratio (–)
λ	thermal conductivity (W/mK)
Γ	surface site density (mol/cm^2)
θ	surface coverage (–)

Subscripts

a	Actual
adb	Adiabatic
avg	Average
in	Inlet
max	Maximum
out	Outlet
W	Wall

Introduction

Combustion using a catalyst is a promising technique to stabilise a premixed flame with low NO_x emission used in a number of applications [1–4] for many years. Recently, research on this technique has been growing with an aim to mitigate greenhouse gas emissions in combustion of hydrogen [5] or hydrogen enriched syngas mixtures [6]. Moreover, hydrogen enriched fuels are now of great interest to replace the fossil fuels in most gas-powered systems [7]. One example is a honeycomb monolith burner [8] consisting of multiple channels used in natural gas fired boiler or turbine applications. In practice, hydrogen non-catalytic combustion in such systems is not simple because of flame instabilities led to incomplete combustion [9,10]. Pizza et al. [9] investigated flame instabilities in a mesoscale planar burner considering heated wall with a hydrogen/air equivalence ratio of 0.5, and varying inflow velocities from 0.003 to 11 m/s. They categorised the instabilities as mild, ignition/extinction, oscillatory, symmetric, and asymmetric based on the flame shapes depending on the inflow velocities. In another study [11], they also discussed the similar flame instabilities in a microscale planar burner where the same inflow conditions were used. A flame can be stable, unstable or blowout in a particular inflow velocity depending on the hydrogen lean composition, as investigated in the experimental work of Schefer et al. [12] in a multi nozzle premixed burner. With an aim to increase the hydrogen/air flame stability, Yang et al. [13] experimentally investigated a converging-diverging tube burner considering various equivalence ratio (0.6–2.2) and inflow velocity (3.4–42 m/s). They found that the flame shape gets thicker and longer with an increased velocity, and the flame stability limit follows an increasing-decreasing trend with the equivalence ratio. However, the tendency to flashback of comparatively rich H_2/Air mixtures limits the applicability of non-catalytic burner due to safety issues. H.Pers et al. [14] experimentally explored possible flashback initiation of H_2/Air laminar flame in a premixed burner and discussed the effects of reactants preheat and wall temperature on flashback. Although some efforts are made considering pin fin arrays [15] and a preheater conductor plate [16] inside the reactor to maintain H_2/Air flame, this is only feasible with high inflow velocity.

In contrast, catalytic aided hydrogen combustion provides a lower activation energy [17], a higher flame stability limit [18], and the potential to reduce NO_x emissions [19]. However, hydrogen catalytic combustion involves complex chemical interactions with solid substrate, resulting in a number of homogeneous (gas phase) and heterogeneous (surface) reactions with increasing temperature [20], and the behaviour of which and impact on NO_x emission are beyond understanding in most applications. Therefore, prior to practical implementation, a comprehensive investigation is required for fundamental knowledge of heterogeneous kinetics and their coupling with corresponding homogeneous kinetics. Many studies have aimed at investigating hydrogen hetero-/homogeneous combustion in a planar burner because of its design simplicity and operation. For example, Appel et al. [21] experimentally investigated the hydrogen/air mixtures over platinum in a planar burner under fuel lean stoichiometric

condition (0.28–0.32), providing results of the onset of homogeneous ignition at different laminar inflow operations. In the same study they numerically studied several hetero-/homogeneous reaction schemes (four homogeneous and three heterogeneous) and addressed the effect of various combination of chemistry coupling. To observe the effect of catalytic reactivity (A_s), Pizza et al. [22] numerically studied a 1 mm height microchannel with an equivalence ratio of 0.5. The results suggest that the catalyst loading controls the mode of combustion and an active catalyst is required to suppress undesirable flame. Similarly, Choi et al. [23] investigated a platinum catalytic micro planar combustor for a range of inflow conditions at stoichiometric H_2/Air mixtures. They found that the platinum catalyst concentration has no effect on reaction characteristics. However, the requirement of a catalyst depends on the specific fuel and catalyst type discussed in the previous study [22]. Again, H_2 combustion using a catalyst is influenced by the wall thermal condition [24]. With an aim to improve hydrogen conversion rate, Y. Zhang et al. [24] investigated catalytic microchannel by varying solid wall thermal conductivity and outer wall heat transfer coefficient. They showed that the conversion rate of H_2 is increased with lower wall thermal conductivity and heat transfer coefficient. The same team [25] also studied the self-ignition process of H_2/Air in microchannel catalytic considering radiation and convective heat dissipation. They showed that the self-ignition process is influenced by several factors which are dependent on temperature. Again, Sui et al. [26] studied combustion stability limits of hydrogen/air mixtures (equivalence ratio = 0.4) in platinum-coated microchannels by considering radiation heat transfer and solid heat conduction. They showed that lower solid thermal conductivity provides wider combustion stability and radiation heat loss towards inlet has a substantial effect on lowering wall temperature.

H_2/Air premixed combustion in a catalytic planar burner has been carried out at elevated pressures. Mantzaras et al. [27] experimentally and numerically studied a hydrogen/air planar combustor with a pressure range of up to 10 bar and found homogeneous combustion suppression at high pressure (>4 bar) due to produced water that acts as a third body efficient radical for terminating gas phase reactions. Moreover, Ghermay et al. [18] investigated the same burner with preheat to gain a better understanding of the pressure/temperature dependence and catalytic chemistry coupling effect. Over the operating conditions considered, the results showed that the mass transport limited conversion of hydrogen and homogeneous combustion could be sustained at high pressure with preheating. Furthermore, the effect of hetero-/homo-geneous chemistry of hydrogen/air combustion in planar burner was studied by considering catalytic segmentation [25,28], burner aspect ratio [29,30], multiple channel [31], and addition of intermediate and final product on homogeneous combustion [32,33]. Besides, Zhang et al. [34] studied a planar model with platinum catalyst and obtained the critical range of equivalence ratio for transitioning from coupling chemistry reaction to pure catalytic/heterogeneous reaction. In another study [24], they investigated the effect of wall thermophysical conditions on hydrogen catalytic reaction and compared the performance in terms of the reaction efficiency and flame stability, which were favourable at higher wall thermal resistance. Similarly, the recent experimental work of Lu et al. [35] reported that the wall heat loss has a significant effect on catalytic reaction. Additionally, they studied the critical equivalence ratio of transformation of reaction type (pure catalytic and hetero-/homo-geneous reaction) for an equivalence ratio range of 0.2–1.2. Hence, the mode (or type) of reaction inside a catalytic burner is highly influenced by the wall thermal conditions. However, an exploration is required to observe the effect of inflow velocity on transforming the reaction type (pure catalytic and hetero-/homogeneous reaction) inside a catalytic burner.

As discussed above, a catalytic combustor of planar type was of prime interest in most studies as it provides efficient interaction with fuel species as well as design flexibility in various applications. Again, the low flame temperatures in such system are vital for zero NO_x emission. For this, the ultra-lean mixtures are preferable, however, there are limited investigations on it. The underlying physics of flame at an ultra-lean condition is to be investigated to get a full understanding of NO_x reduction process. Moreover, wall thermal condition in a planar burner was considered convective heat loss or fixed temperature in previous studies but an adiabatic assumption is more practical for modelling a multi-channel honeycomb burner as heat is uniformly distributed in this case. Hence, the heat conduction in solid wall has not been considered in the present study. Furthermore, a flame stability analysis is necessary for this condition to observe the challenges prior to switching to catalytic approach.

The present work undertakes a numerical study on both non-catalytic and catalytic planar models for hydrogen/air combustion. The computations on two-dimensional laminar flow species transport model with multicomponent diffusion were carried out. Both homogeneous and heterogeneous kinetics were included in species transport modelling. A stability map as a function of Reynolds number for homogeneous combustion under fuel lean operation of equivalence ratio of 0.18 and 0.20 was obtained. The objectives were to assess the gas phase stability map and to delineate the catalytic approach for hydrogen/air combustion with NO_x emission over a range of equivalence ratio (0.10–0.20).

The article is organised as follows. First, the numerical model of planar burner is validated with experimental measurements. Then a stability map is obtained and discussed for homogeneous combustion in non-catalytic burner. Transition of chemistry coupling in catalytic burner, and their effects are analysed with species average mole fraction profiles, average temperature profiles and contour plots. Finally, NO_x emission chrematistics are discussed.

Computational modelling

Fig. 1 shows a schematic of a planar burner having a dimension of $h = 7$ mm between two parallel Pt coated plates. The chemically reacting gas flow through the burner is governed by the Navier-Stokes, energy and species transport equations which are solved considering steady-state, laminar and multicomponent flow assumptions. The equations solved are stated as follows:

Continuity equation:

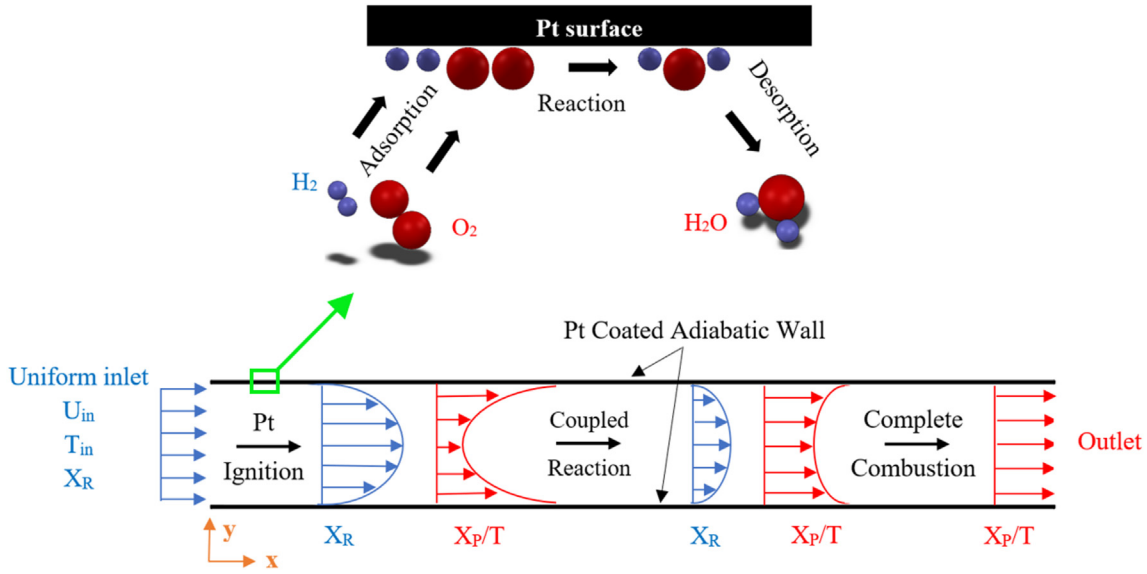

Fig. 1 – Schematic of the catalytic burner geometry (L – burner length, h – gap between wall).

$$\nabla.(\rho \mathbf{u}) = 0 \tag{1}$$

Where ρ is the density, $\mathbf{u}$ is the velocity vector.

Momentum equations:

$$\nabla.(\rho \mathbf{u}\mathbf{u}) = \nabla.\mu\left[\nabla\mathbf{u} + (\nabla\mathbf{u})^T - \frac{2}{3}(\nabla.\mathbf{u})I\right] - \nabla p \tag{2}$$

where μ is the dynamic viscosity, p is the pressure, I is the unit tensor.

Energy equation:

$$\nabla.(\mathbf{u}(\rho e + p)) = \nabla.\left(\lambda\nabla T - \sum_{i=1}^{n} h_i \mathbf{J_i} + \tau.\mathbf{u}\right) \tag{3}$$

where e, T, λ, h_i, J_i and τ denote the total energy including pressure work and kinetic energy, temperature, thermal conductivity, species enthalpy, species diffusion flux and viscous stress tensor, respectively. Here, n is the total number of gas species (i).

Species transport equations:

$$\nabla.(\rho \mathbf{u} Y_i) = -\nabla.\mathbf{J_i} + R_i \tag{4}$$

Here, Y_i is the species mass fraction. The species diffusion fluxes (J_i) are computed from the multicomponent diffusion equations of Maxwell-Stefan [36] considering the thermal diffusion for light species. The source term, R_i is the result of the rate of production and destruction of gas species (i).

Surface species coverage equations:

$$\frac{d\theta_j}{dt} = \frac{s_j}{\Gamma} = 0 \; (j = 1, 2, \ldots\ldots, m) \tag{5}$$

Where θ, s and Γ are the surface species coverage, surface species molar production rate and surface site density, respectively. The alteration of species site coverage that is a fraction of the surface sites covered by species (j) calculated from the above equation (5). The production rate (s) for each surface species is computed considering both gas and surface species' production and destruction by the surface reactions. Here, m is the total number of surface species (j). At the steady-state condition, the transient term of the equation vanishes and the net production rate equals to zero.

The boundary condition for burner wall is considered to be no slip and adiabatic. The interfacial gas-wall boundary ($y = 0$ and $y = h$) conditions for gas-phase species are $(\rho Y_i V_{i,y})_y = W_i s_i$. Where V_i, W_i, and s_i are the gaseous species diffusion velocity, molecular weight and heterogeneous molar production rate, respectively. Inflow boundary conditions are set uniform for velocity, temperature, and the species mass fraction. A zero gradient boundary condition is imposed at the outlet for all the properties and the pressure is specified as atmospheric. To simulate the radiation effects between the inner surfaces, at the inlet and outlet, the discrete ordinates (DO) model is used. The DO radiation model is uncoupled, in which energy iterations per radiation iteration is set to 10. The radiation heat transfer from a hot reaction zone towards the inlet and outlet are considered at boundary temperature. The internal emissivity of 1.0 is set for Pt-coated surface, the inlet and outlet enclosures. The Pt catalyst wall acts as an igniting medium of the incoming premixed H_2/air mixture, releasing radicals and heat that promote the gas phase reaction. H_2/air lean mixtures (varying $\varphi = 0.10–0.20$) are considered at the inlet temperature of 312 K. Such flow conditions are chosen to represent a range of low temperature heating applications, covering the inflow velocity from 0.075 m/s to 3.5 m/s at 1 atm. These conditions can be characterised by the flow Reynolds number based on the burner height ($h = 7$ mm). The upper limit of the Reynolds number studied is 1333 which is below the critical Reynolds number 1400 and thus justifies the laminar assumption in the present configuration.

The above governing equations were discretized and solved on a structured grid using Finite Volume Method (FVM). The grid with 350 × 100 points (in the x axis and y axis, respectively) over the burner domain (250 mm × 7 mm) was

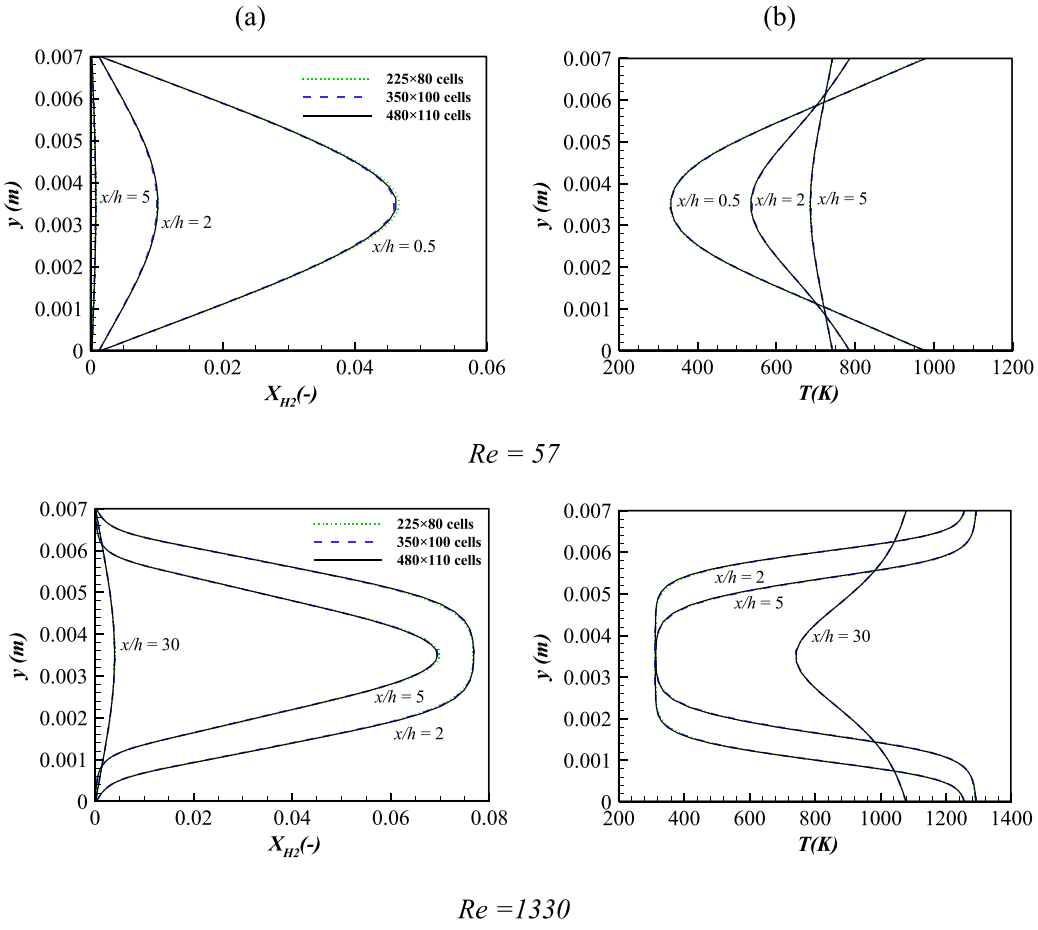

Fig. 2 – Grid test: Transverse profiles at three selected streamwise locations, (a) hydrogen mole fraction (X_{H2}) (b) Temperature (T), φ = 0.20, T_{in} = 312 K.

sufficient to obtain a grid independent solution. Grid towards the inlet and walls were refined to capture the high gradients of flow variables. The near upstream node and near wall node were positioned at *x*/*h* (from inlet) = 0.033 mm and *y*/*h* (from catalytic wall) = 0.0061 mm, respectively. An example of grid test is presented in Fig. 2 which ensures the grid requirement for the Reynolds number from 57 to 1333. However, the burner length in this study was also extended up to 700 mm for capturing the entire reaction zone at higher Reynolds numbers of interest. As a result, a total of 900 × 100 grid points in the extended domain was used keeping the same resolution near upstream and also at the near wall region. Ansys Fluent 2020 R2 version was used to carry out computations. A 2-D double precession planar steady-state solver was selected, and viscous model was set to laminar. Species transport model was used to solve the volumetric and wall surface reactions using a stiff chemistry solver with finite rate chemistry. For pressure velocity coupling, SIMPLE algorithm was used. Spatial discretization method for the gradients and pressure were specified as least square cell based and second order, respectively. To ensure accuracy, momentum, energy, and species equations were spatially discretized with a second order upwind method. The simulation terminates when the convergence criteria of 10^{-6} for all the residuals were met or the residuals approach steady states.

Chemical kinetics

A detailed mechanism of surface reactions [37] for hydrogen oxidation over the platinum catalyst, was used in this study. The mechanism consists of eleven irreversible and three reversible reactions and, has five surface and six gaseous species. The platinum surface site density (Γ) was set to 2.7×10^{-9} mol/cm^2 [37]. The homogeneous gas phase chemistry proposed by Warnatz et al. [38] was used with the heterogeneous surface chemistry, which includes nine species and nineteen elementary reactions. CHEMKIN [39] and Surface-CHEMKIN [40] were used to calculate the homogeneous and heterogeneous reaction rates, respectively, while the transport properties were evaluated from the CHEMKIN transport database [41]. Furthermore, to simulate NO_x emission, a NO_x kinetic scheme is added to gas phase kinetics for the catalytic burner. As mentioned in many studies, NO_x in H_2/air combustion comes mainly from NO and NO_2. NO can be produced in three ways: the thermal route using Zeldovich mechanism [42], the N_2O route and the NNH route [43]. The thermal NO is significant in high flame temperature combustion which is available in the Ansys Fluent module and estimated at post-processing stage. The kinetics of the N_2O route and NNH route are taken from Glarborg et al. [43] and are considered responsible for NO_x emission over a wide range of

lean combustion. The well-established NO_2 reaction of Howard et al. [44], is considered to estimate NO_2. However, the mixture gas viscosity and thermal conductivity were computed using mass weighted mixing law. Both the multicomponent and thermal diffusions were considered in the simulation and the kinetic theory was used for the calculation of binary mass diffusion coefficients and thermal diffusion coefficients.

Validation of the numerical simulations

In order to validate the numerical model, the computed results are compared against the existing experimental results [21]. The burner configuration chosen was the same as experiment [21]. Inflow parameters from the experiment were copied exactly in simulation and the measured temperatures along the burner length were used as a wall boundary condition. An extensive validation was carried out at different flow conditions and, the profiles of species mole fraction as well as temperature in five axial locations were compared. An example of validated results for $\varphi = 0.28$, $T_{in} = 312$ K, $Re = 762$ is shown in Fig. 3(a). The overall agreement between the measured and computed results is excellent and the maximum deviation is estimated only less than 3%. Besides, a comparison of the onset of homogeneous ignition is also presented in terms of the OH contour plot in Fig. 3(b) which further confirms the accuracy of the numerical model used in the work.

Results and discussion

A stability map of the fuel lean H_2/air combustion in non-catalytic burner is firstly presented, to gain a comprehensive understanding of the challenges and also to facilitate the discussion of the importance of using a catalyst under similar operating conditions. Then, a comparison is made between pure catalytic and coupled chemistry (hetero-/homogeneous reactions). Finally, NO_x emissions are computed.

Flame stability map in non-catalytic burner

The flame stability map of premixed fuel lean H_2/air is shown in Fig. 4(a). The computations of fuel lean conditions were performed under wall adiabatic condition by varying the inflow Reynolds number (*Re*). The φ for H_2/air is considered here just above the lower flammability limit from 0.15 to 0.20. Prior to combustion, the H_2/air mixtures is ignited on both surface wall at a distance 0.5*h* from inlet. The ignition temperature is set equal to adiabatic temperature of respective stoichiometric condition. The average outlet temperature ($T_{out,avg}$) (Left axis) of products and the dimensionless heat loss at the inlet (Q_{loss}/HoR_a) (1st right axis) and unburned H_2(%) (2nd right axis) exiting the burner outlet are presented as a function of *Re*. Here, Q_{loss} is defined as the net heat leaving the burner through the inlet and calculated from the following expression:

$$Q_{loss} = Q_{rad} - H \tag{6}$$

Where Q_{rad} and H are the radiation heat and enthalpy flux through the inlet boundary, respectively. Q_{loss} is made dimensionless with the actual heat of reaction (HoR_a) inside the burner. The dashed and solid lines denote the results of the equivalence ratio (φ) of 0.18 and 0.20, respectively. It should be noted that for $\varphi \leq 0.16$ no flame is observed under the present operating conditions, but the flame extinction lower limit for $\varphi = 0.18$ and $\varphi = 0.20$ is found below $Re < 571$ and $Re < 381$, respectively as pointed out by the arrows in the temperature results. $T_{out,avg}$ measured both cases gradually increases with *Re* and this variation is due to the unburned H_2 exiting the burner and the radiation heat loss at the inlet. At a low *Re*, high radiation heat loss causes a low flame temperature in the reaction zone and consequently, less H_2 conversion. The maximum unburned H_2 at the near flame extinction limit is obtained 11.5% and 10.3% for $\varphi = 0.18$ and $\varphi = 0.20$, respectively. Again, as the *Re* increases, the radiation heat loss gradually decreases. Therefore, there is increased flame temperature with *Re*. However, the flame extinction higher limit is not obtained within the *Re* studied here.

Fig. 4(b) shows average mole fraction (Left axis) of H_2 and H_2O, and average temperature (Right axis) for $\varphi = 0.20$ along the burner length (*x*/*h*). Solid line and dashed line denote the results of $Re = 762$ and $Re = 1333$, respectively. The OH mole fraction on the wall shows the onset position where the flames are ignited. As shown, the flame ignition for both *Re* is almost at the same position and, precisely within 0.20–0.30 of *x*/*h*. T_{avg} increases up to a certain burner length as a result of the high rate of H_2 consumption, then decreases to a constant value. As expected, the trend of $X_{H2O,avg}$ is similar. However, the position at which the flame peak temperature occurs is varied respectively at $x/h = 10$ and $x/h = 14.3$ for $Re = 762$ and $Re = 1333$. The interesting point is that there is no change in $X_{H2,avg}$ beyond the position of the flame peak temperature for both cases. The reason is the position of reaction zone attached to the wall keeping H_2 unburned in the burner centre region as shown in Fig. 5(a). As the results indicate, most of H_2 is consumed within the reaction zone and after that no further reaction of H_2 takes place. Again, the peak temperatures exceed the adiabatic flame temperature ($T_{adb-} = 937$ K) and are pronounced near the wall of the burner. This is because of diffusional imbalance of the H_2/air mixture as the Lewis number of H_2 is below unity (i.e. $Le = 0.3$). Therefore, the H_2 species high affinity towards the hot reaction zone causes a comparatively rich mixture and high temperature. To get a better understanding of the reaction zone, the temperature contour plots are shown in Fig. 5(b) for three different *Re*. As the main interest is on the reaction zone near upstream, only 3/7 of the burner length is presented. The high temperature region near the wall is the reaction zone and the shape of the zone is symmetric about the burner mid plane. At low $Re = 381$, the reaction zone is confined to a small region near upstream. As *Re* increases, the reaction zone elongates along the burner length. Such behaviour was also predicted in the same burner by Pizza et al. [9] but at different inflow conditions ($\varphi = 0.50$ and $1110 < Re < 2960$), and they defined the flame as an open symmetric steady flame. However, it is worth noting that complete H_2 conversion is not attained at the burner exit under the current operating condition.

Catalytic burner combustion

To investigate the catalytic effect in the same burner, the wall is considered as a Pt coated reacting surface, and the

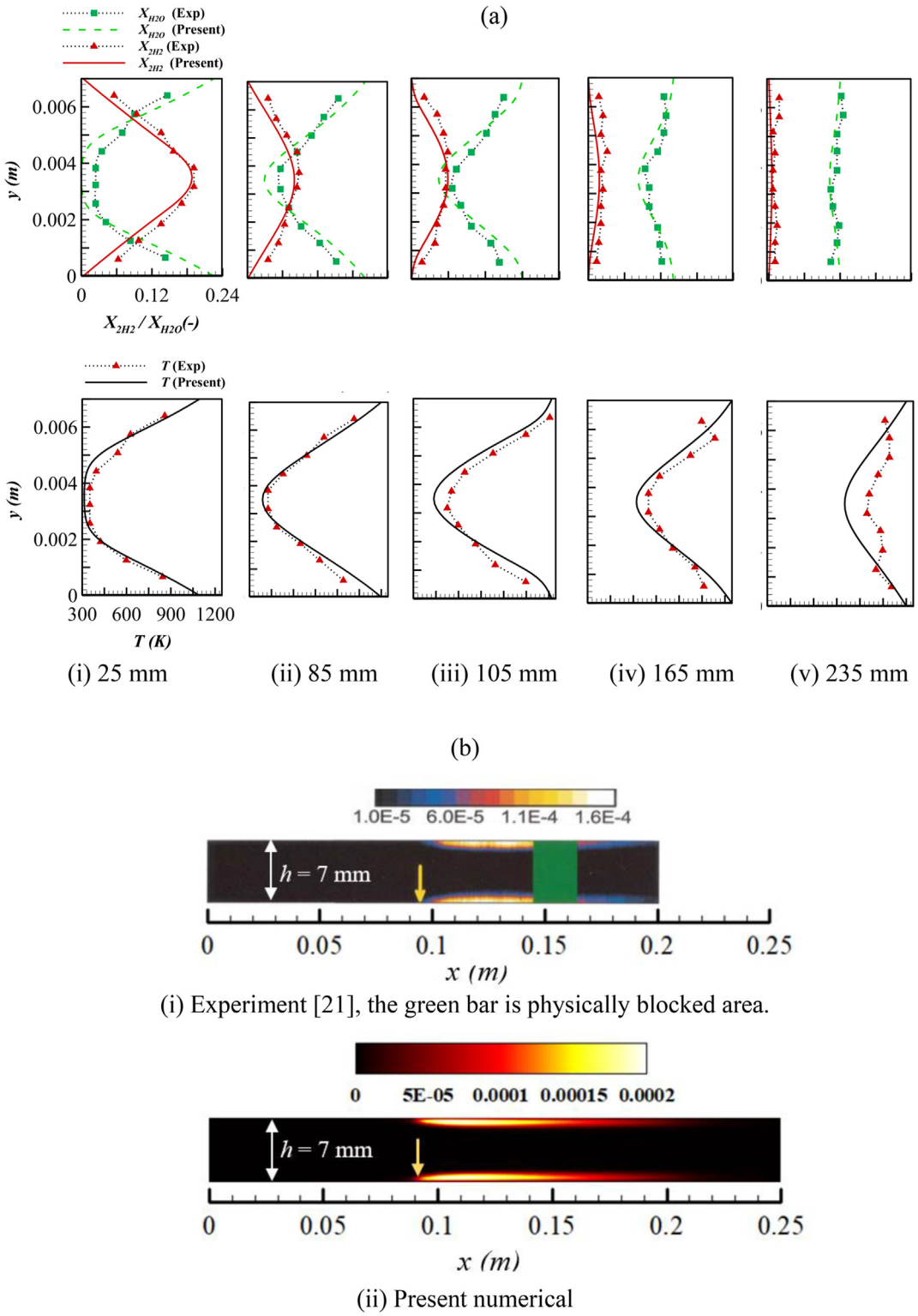

Fig. 3 – Comparisons of (a) species and temperature profiles at axial positions (b) OH contour plot (arrow indicates the onset of homogeneous ignition), $\varphi = 0.28$, $T_{in} = 312$ K, Re = 762.

elementary chemistry of Deutchmann et al. [37] is implemented including the gas phase chemistry. The other boundary conditions are kept similar as in the non-catalytic burner.

Flame stability

Fig. 6 shows the OH contours inside the catalytic burner at different operating conditions. The results are presented for four equivalence ratios (φ) of 0.10, 0.15, 0.18 and 0.20. H_2

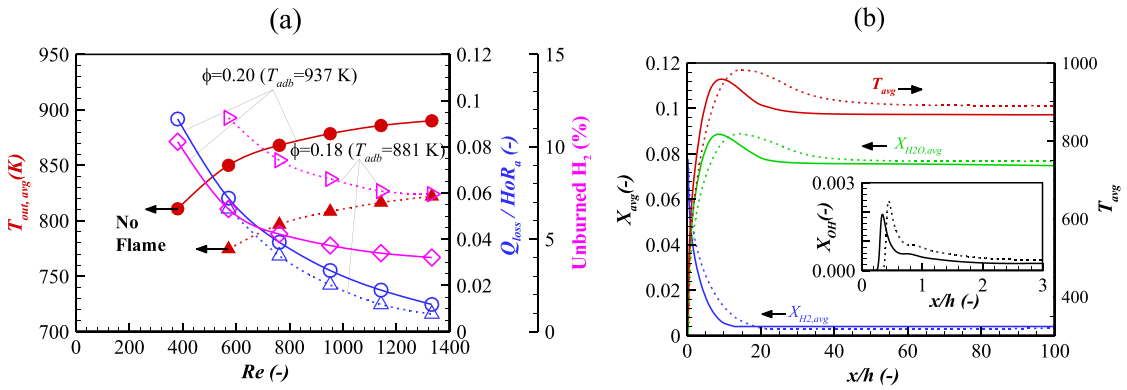

Fig. 4 – H_2/air combustion in non-catalytic burner (a) stability map as a function of Re (b) Average value along the burner length (φ = 0.20, T_{in} = 312 K): Left Axis- Mole fraction (X_{avg}); Right Axis- Temperature (T_{avg}). OH mole fraction is taken on surface wall. Re = 762 (solid line); Re = 1333 (dashed line).

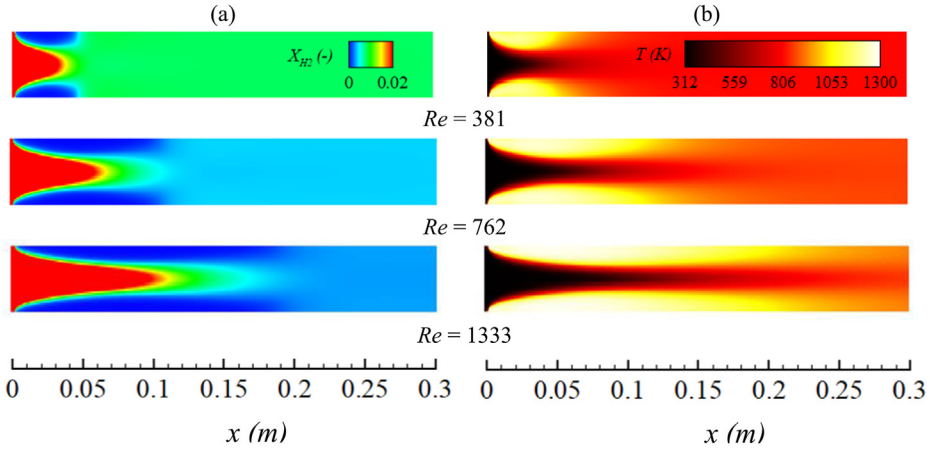

Fig. 5 – Contour plots at different Reynolds numbers inside non-catalytic burner for φ = 0.20, T_{in} = 312 K (a) hydrogen mole fraction (X_{H2}) (b) Temperature (T).

conversion is achieved 99.9% at the burner exit almost in all the cases except in a few cases where $\varphi = 0.10$ at high Reynolds number. Only the X_{OH} contour plot of $x/h = 30$ is shown to focus the interest. The X_{OH} scale is kept 0-10^{-4} to capture the onset of homogeneous combustion. The equivalence ratio of $\varphi = 0.10$ represents an ultra-lean mixture as that is below the lower flammability limit of hydrogen. For this case, no significant X_{OH} is observed over the range of *Re* considered, which indicates pure catalytic conversion of H_2. At a near flammability limit ($\varphi = 0.15$), the flame is ignited near the burner wall at $x/h = 10$ when *Re* is 571. However, as *Re* increases, the onset position remains approximately the same, and the flame shape is elongated along the burner length. Whereas, at a lower $Re < 571$, flame is not ignited because of the high radiation heat loss at the inlet as shown in Fig. 7 (a). Under such conditions, pure catalytic (i.e., heterogeneous) chemistry (PC) plays the main role in complete H_2 combustion, which will be discussed in more details in the later section. Again, flame ignition occurs at a lower $Re = 381$ for $\varphi = 0.18$ and the onset position shifts toward the inlet. This is due to the comparatively rich H_2/air mixture closer to the upstream near catalytic surface and releases high heat promoting flame ignition. This effect is also observed for $\varphi = 0.20$ where the onset position is very close to the inlet.

Fig. 7 (a) shows the dimensionless heat loss (Q_{loss}/HoR_a) (right axis) at the inlet and the convective heat (*H*) (left axis) as a function of *Re*. The heat loss is dependent on φ as the radiating temperatures are different. At a low *Re* for all φ, the heat loss is very high and then gradually decreases with *Re*. However, the heat loss becomes negative at high $Re > 952$ cases for $\varphi = 0.10$. This is because *H* dominates over Q_{rad} at the inlet, and thus the (Q_{rad} - *H*) becomes negative which further indicates no heat leaving the burner inlet. As expected, the convective heat increases with *Re* and is independent on φ. As also mentioned earlier, the radiation heat loss through inlet has a significant influence on the flame temperature and reaction kinetics. However, the average flame outlet temperatures ($T_{out,avg}$) with increasing *Re* for catalytic combustion are shown in Fig. 7 (b). The arrow denotes the transition of pure catalytic chemistry (PC) to coupled (hetero-/homogeneous) chemistry (CC) reaction.

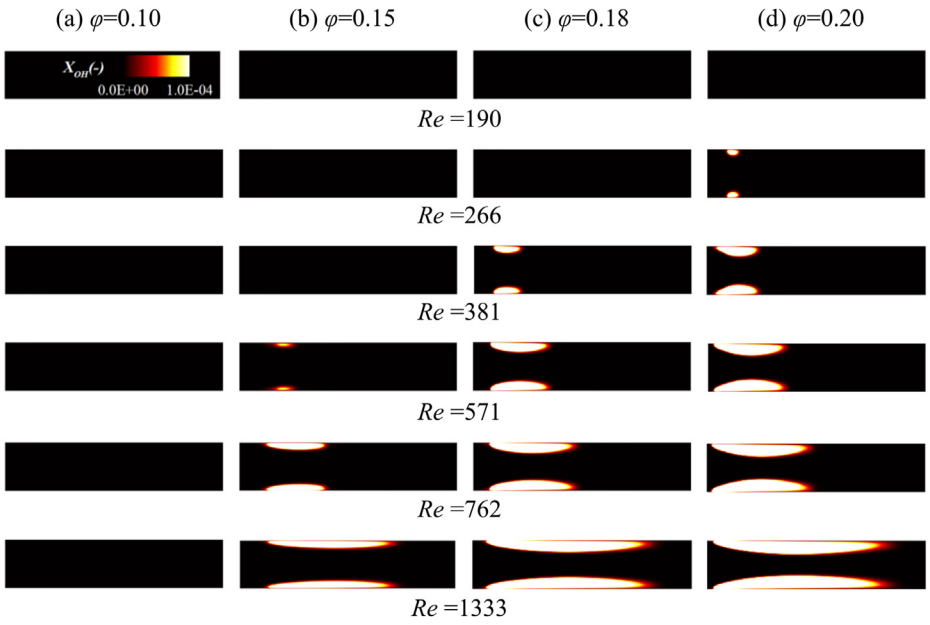

Fig. 6 – OH contour plot inside catalytic burner (up to *x/h* = 30) at different *Re*, T_{in} = 312 K.

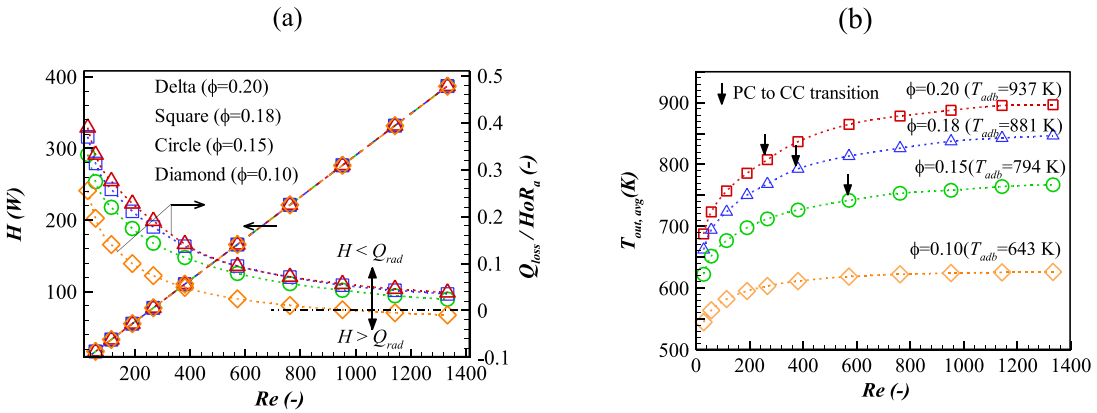

Fig. 7 – Catalytic burner: (a) Left axis: Enthalpy flux at inlet (*H*), Right axis: Net heat loss at inlet (Q_{loss}/HoR_a) (b) Average outlet temperature ($T_{avg,out}$), T_{in} = 312 K.

Effect of coupled (hetero-/homogeneous) chemistry

The distribution of species mole fraction and temperature on the catalytic wall are shown in Fig. 8 for φ = 0.20. To identify the effect of the homogeneous chemistry on catalytic combustion, two Reynolds numbers, 190 and 762, are selected for comparison where the pure catalytic chemistry (PC) and coupled chemistry (CC) are dominant, respectively. At the pure catalytic mode, the computation is performed without considering the homogeneous chemistry. Fig. 8 (a) shows a comparison of the results of PC (dashed line) and CC (solid line) for Re = 190. There is no variation observed in the species mole fraction of H_2, H_2O and OH and wall temperature (T_W). The catalytic conversion starts at the beginning of upstream wall resulting in a high temperature near upstream close to the wall. Then, it decreases as there is gradual reduction of H_2 concentration along the length. T_W becomes steady where no unburned H_2 is left.

Similarly, no changes between the two chemistries are found in the surface coverages as shown in Fig. 9 (a), where PT(s) and O(s) constitute the main coverage. Here, the surface coverage is the fraction of surface sites covered by species and PT(s) is available surface sites for adsorption. O_2 adsorption/desorption has strong dependence on the wall temperature as discussed in the earlier studies [37,45]. As the temperature decreases, the excess O_2 allows for O_2 adsorption that consequently promotes H_2 reaction. Therefore, H_2 is completely consumed. The available uncovered surface sites PT(s) are then used for further O_2 adsorption. However, all the results indicate that the contribution of the homogeneous chemistry on the species concentration is negligible for *Re* = 190. By comparison, the effect of homogeneous chemistry is significant for *Re* = 762 shown in Fig. 8 (b). The X_{H2} distribution on the wall for PC decreases gradually but the distribution for CC is very low and, approaches zero within a certain burner length.

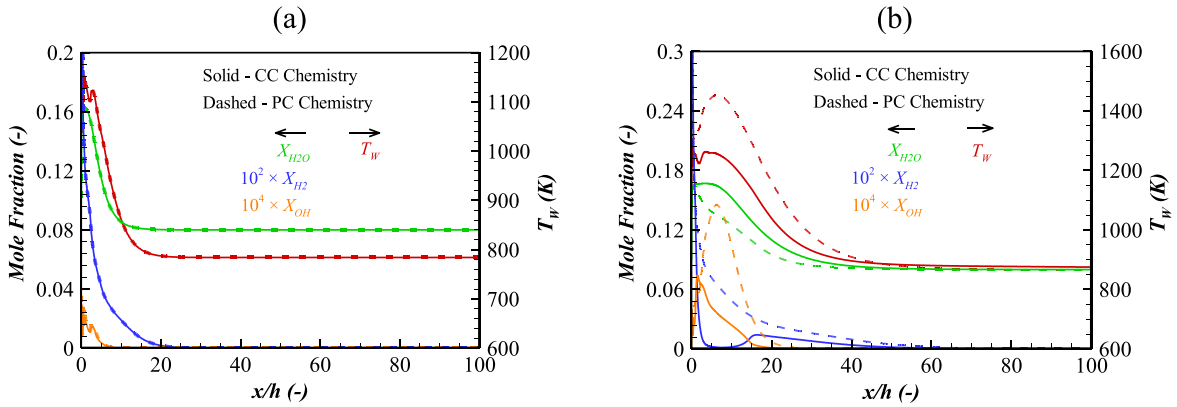

Fig. 8 – Comparison of species mole fraction and temperature distribution on wall between Coupled (CC) and pure catalytic (PC) chemistry, $\varphi = 0.20$, $T_{in} = 312$ K (a) $Re = 190$, (b) $Re = 762$.

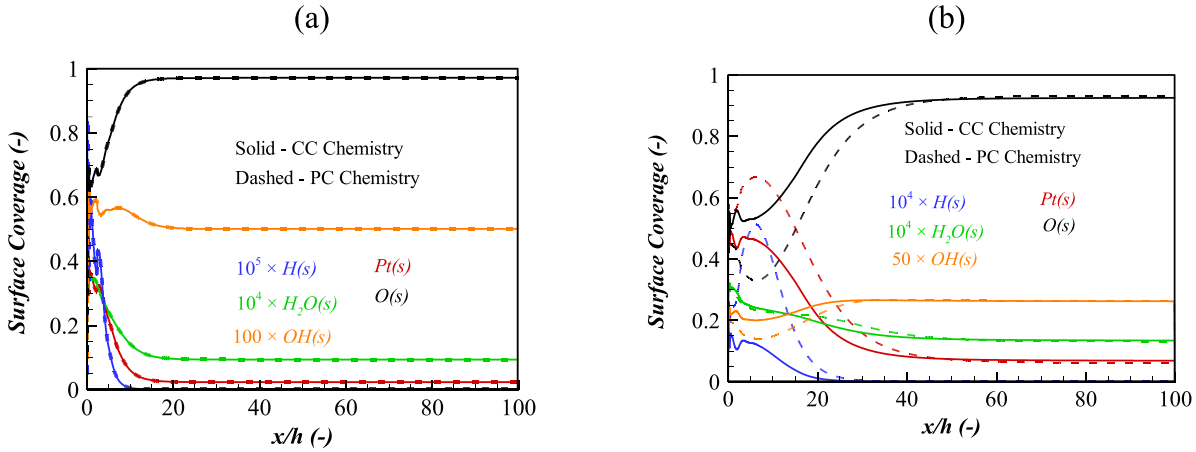

Fig. 9 – Comparison of species surface coverage on wall between Coupled (CC) and pure catalytic (PC) chemistry, $\varphi = 0.20$, $T_{in} = 312$ K (a) $Re = 190$, (b) $Re = 762$.

This is due to the homogeneous reaction zone in proximity to the catalytic wall. Therefore, most of H_2 near the surface is burned in the reaction zone, reducing the H_2 level on the catalytic surface. Consequently, the H_2O wall distribution for CC is found to be higher. However, the X_{OH} distribution on the wall is lower for CC because of the strong influence of the catalytic reaction. Previous studies [21,46] showed that the catalytic reaction influences the homogeneous ignition as the catalyst itself produces less OH. So, catalyst is an efficient sink of homogeneously produced OH inhibiting homogeneous reaction. Moreover there is significant variation of wall temperatures between two chemistries (PC and CC) which is discussed in later section. A comparison of the surface coverages for $Re = 762$ is shown in Fig. 9 (b). As expected, there is a large variation in the surface coverage values near the homogeneous reaction zones. The hydrogen adsorption H(s) for CC is found to be less as there is high H_2 consumption in the reaction zone. For example, the maximum variation between two chemistry (CC and PC) is at a distance $x/h = 7.7$ from inlet where temperature difference is maximum. Here, the H(s) ($\times 10^4$) level for CC and PC are 0.11 and 0.48, respectively. Again, the OH adsorption in CC is higher due to the influence of the catalytic reaction. At $x/h = 7.7$, the OH(s) ($\times 50$) level for CC and PC are 0.202 and 0.141, respectively. However, there is no significant variation observed in H_2O(s) at that position.

Surface temperatures

The maximum surface temperature, T_W, in all cases depicted in Fig. 10, exceeds the adiabatic flame temperature. This is due to the diffusional characteristics of the H_2/air mixture which

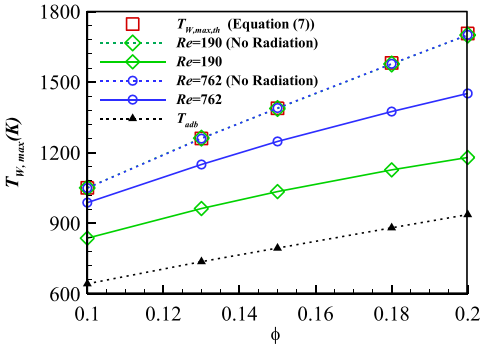

Fig. 10 – Maximum wall temperature using pure catalytic chemistry (PC), $T_{in} = 312$ K.

can be described by the theoretical wall temperature ($T_{w,max,th}$). In the case of the catalytic surface reaction on a flat plate, it is shown in Ref. [47] that $T_{w,max,th}$ remains constant along the plate under adiabatic conditions and is determined as:

$$T_{w,\max,th} = T_\infty + Le_{H_2}^{-2/3}(\Delta T) \quad (7)$$

where Le_{H_2} is the hydrogen Lewis number and its value of 0.30 is considered in all the cases, T_∞ is the free stream temperature, and ΔT is the combustion temperature rise from the adiabatic temperature:

$$\Delta T = T_{adb} - T_\infty \equiv Y_{H_2,\infty} Q_{H_2} / C_p \quad (8)$$

Here, T_{adb} is the adiabatic flame temperature, Y_{H_2} is the free stream hydrogen mass fraction, Q_{H_2} is the combustion heat per unit mass of hydrogen. At a unity Lewis number, the H_2/air flame temperature is identical to the adiabatic temperature but it always becomes super-adiabatic temperature ($T_{w,max,th} > T_{adb}$) at a Lewis number less than unity. Fig. 10 shows the maximum wall temperature using the pure catalytic chemistry (PC) for $0.10 \leq \varphi \leq 0.20$ along with $T_{w,max,th}$ calculated from equation E7. The computed maximum wall temperatures ($T_{W,max}$) for the Reynolds numbers of 190 and 762 are shown, considering with and without radiation. The $T_{W,max}$ values are identical to $T_{w,max,th}$ irrespective of the Reynolds number when the radiation model is not included. With radiation, the predicted catalytic peak temperatures are lower than the theoretical value due to the radiative heat loss towards the inlet. In particular, at a lower $Re = 190$, the $T_{W,max}$ are comparatively very low because of the high heat losses at the inlet discussed in Fig. 7.

However, the wall temperature for CC in Fig. 8 is lower than PC in the region of homogeneous reaction zone. This is because of the shielding effect of the homogeneous reaction zone that limits the surface superadiabaticity induced by the catalyst [27]. Furthermore, there are up/down peaks on the wall temperature near inlet as shown in Fig. 8. These peaks are mainly from the effect of radiation. To observe this effect, the incident radiation (G) and net radiation heat flux (q_{rad}) at the inlet and on the wall surface are presented in Fig. 11. At the inlet, Fig. 11 (a), the incident radiation is maximum at the wall and then gradually deceases to a minimum at midplane for $Re = 762$. For $Re = 190$, the minimum occurs at y/h ≈ 0.15 at a distance from bottom wall (which is the same in case of top wall because of symmetry) and then reaches to peak at y/h ≈ 0.20. Apart from that there is no significant variation. The magnitude between two Re differs significantly as the amount of fuel burned is different. However, the radiation heat fluxes have significant variation within y/h ≈ 0.20 from the bottom wall for both cases ($Re = 190$ and 762). Again, the trend and magnitude are approximately similar. The plot for $Re = 762$ shifted toward wall is expected as the net heat loss for both cases are not same. Here, it should be noted that the negative heat flux represents the radiative heat flux leaving the burner whereas the positive value is the opposite.

However, the up/down peaks of incident radiation are observed on surface wall near upstream within the burner length (x/h) of 5 for both cases. This is the effect that causes the up/down peaks of the wall temperature near upstream (Fig. 8) and consequently affects the reaction kinetics on the catalytic wall (Fig. 9). After $x/h > 5$, the incident radiation decreases gradually without showing any variation. Consequently, the radiation heat fluxes are maximum at inlet and then decrease along the length. This becomes negative within the range 5 ~20 and 15 ~40 of x/h for $Re = 190$ and $Re = 762$, respectively. This further indicates that the radiation flux directed towards the wall in that region and then, it becomes zero because of the uniform flame temperature.

H_2 conversion

The percentage of H_2 converted for $\varphi = 0.20$ at different Re is shown in Fig. 12 (a) along the length of the burner. The percentage is estimated from the average results at different axial positions of the burner:

$$H_2 Conversion(\%) = \frac{Y_{H2,avg,in} - Y_{H2,avg,x}}{Y_{H2,avg,in}} \times 100 \quad (9)$$

Where $Y_{H2,avg,in}$ is the average H_2 mass fraction at the inlet, $Y_{H2,avg,x}$ is the average H_2 mass fraction at axial positions. For all cases, almost 99.9% H_2 conversion is achieved within the burner length considered in this study. By comparison, the complete H_2 conversion for lower Re is obtained at shorter length because of the higher residence time shown in Fig. 13. The residence time is calculated from the minimum burner

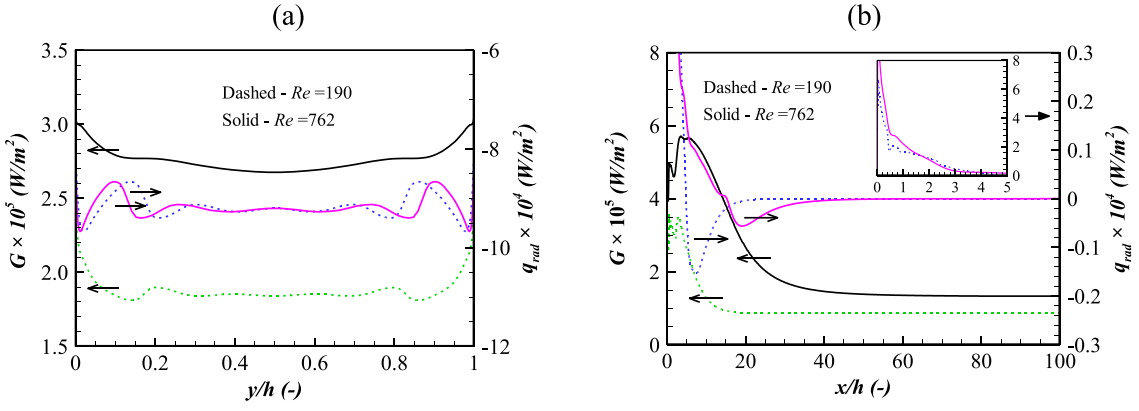

Fig. 11 – Variation of Incident Radiation (Left Axis) and Net Radiation Flux (Right axis), Coupled chemistry (CC), $\varphi = 0.20$, $T_{in} = 312$ K at (a) inlet (b) wall.

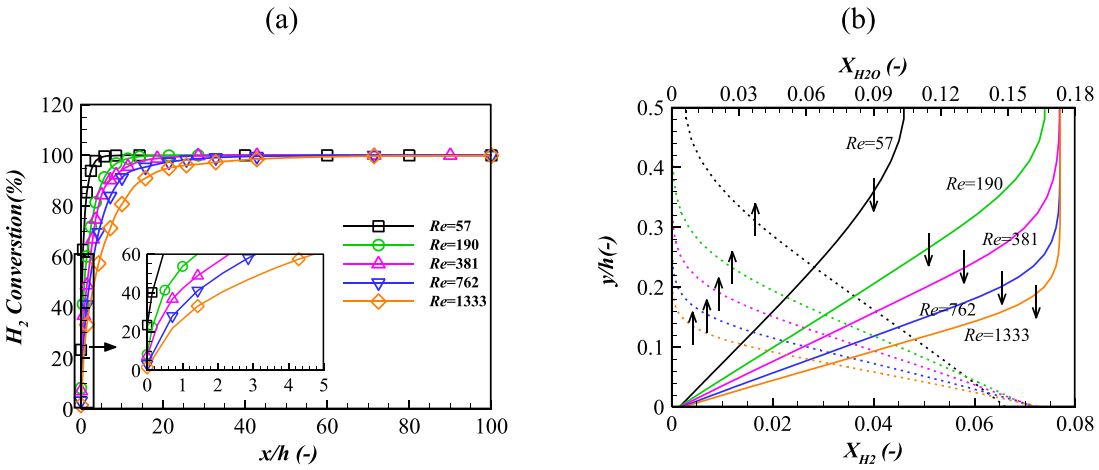

Fig. 12 – (a) H_2 conversion at different *Re*, (b) H_2 and H_2O distribution at x/h = 0.5, Coupled chemistry (CC), $\varphi = 0.20$, $T_{in} = 312$ K.

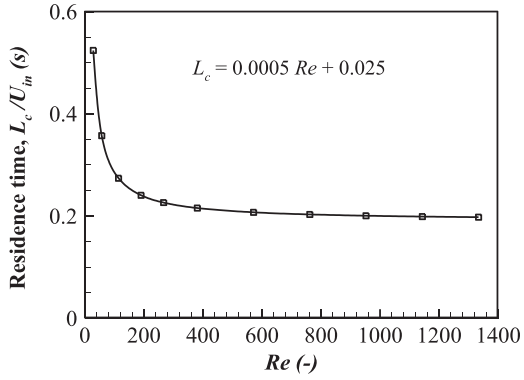

Fig. 13 – Residence Time as a function of *Re* using coupled chemistry (CC), $\varphi = 0.20$, $T_{in} = 312$ K.

length (L_c) for 99.9% H_2 conversion and inflow velocity. For $\varphi = 0.20$, the relation $L_c = 0.0005\ Re + 0.025$ is obtained. However, the zoomed view in Fig. 12 (a) shows a significant catalytic conversion near upstream. For $Re = 57$, the conversion is above 22% at near upstream and, this becomes comparatively less at higher *Re*. The main reason is a high rate of H_2 consumption in the entrance region of the burner. Again, the low inflow and high residence time at a lower *Re* facilitates H_2 diffusion towards the catalytic surface. For clarification, Fig. 12 (b) shows the mole fraction distribution of H_2 and H_2O at $x/h = 0.5$ from inlet. The vertical up and down arrows denote X_{H2O} (dashed) and X_{H2} (solid), respectively. The low H_2 level near wall for all cases indicates that catalytic reaction is practically mass transport limited. However, the H_2 distribution across the burner for $Re = 57$ is low because of the strong H_2 diffusion to the catalytic wall. Consequently, this produces high H_2O (dashed-black). When *Re* increases, the flow becomes convectively dominant and thus reduces the residence time for H_2 diffusion. As a result, the H_2O production is comparatively less with increasing *Re*.

However, H_2 transport toward the catalytic surface is governed by the catalytic reaction, which depletes both H_2 gas and surface species and maintains a mass transfer between two species. In reality, the species boundary layer is developed on the catalytic surface that inhibits the mass transfer. Therefore, the mass transfer coefficient can be used as a measure of resistance to mass transfer between the mean species composition and the composition at the reacting surface. This is a useful approach if the mass transfer coefficient is calculated quantitatively but, for a complex catalytic reacting flow, the mass transfer coefficient cannot be correlated in a simple way. Nevertheless, they can be used qualitatively to predict the catalytic reacting flow using the dimensionless Sherwood number (*Sh*).

$$Sh = \frac{k_c h}{D_m} \tag{10}$$

Where k_c is the mass transfer coefficient and D_m is the mass diffusivity for fuel species (H_2). The expression for k_c is as follows:

$$k_c = \frac{D_m \frac{\delta C_{H2}}{\delta y}\Big|_{y=0}}{C_{H2,W} - C_{H2,m}} \tag{11}$$

As noted in the above equation, $\delta C_{H2}/\delta y$ is the gradient of the species molar concentration at surface. The $C_{H2,W}$ and $C_{H2,m}$ are the surface and the mean concentration of H_2, respectively. The $C_{H2,m}$ is transversely calculated from the following equation.

$$C_{H2,m} = \frac{\int_0^h C_{H2} u dy}{\int_0^h u dy} \tag{12}$$

In this equation, *h* is the burner height, *u* is the local velocity and C_{H2} is the local molar concentration of H_2. Fig. 14 shows the computed axial Sherwood number of H_2 species for three different *Re*. As expected in all the cases, *Sh* have high initial values near upstream, which are associated with the

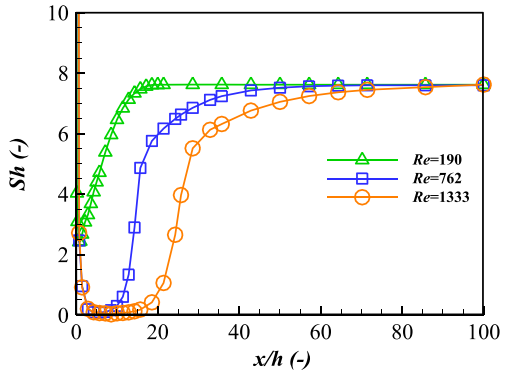

Fig. 14 – Local Sherwood Number (Sh) along the burner length for H_2, Coupled chemistry (CC), φ = 0.20, T_{in} = 312 K.

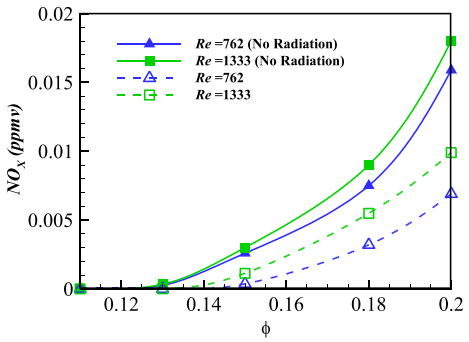

Fig. 16 – NO_x Emission as a function of φ using coupled chemistry (CC), T_{in} = 312 K.

very thin H_2 boundary layer developed at the leading edge of the catalyst. This sharply decreases to a minimum value ~3.0 at x/h = 2.0 for Re = 190, and then, increases to an asymptotic value of around 7.6 at x/h = 20, indicating no significant catalytic activity beyond this length. The behaviour of sharp decrement in the near inlet region is due to the high temperature differences between the wall and bulk temperature, which significantly affects the property of light species like H_2. Previous studies [48] showed such effect of temperature on the H_2 properties and other dimensionless quantities inside a pipe for non-reacting flow.

NO_x emission

The NO_x emission for ultra-lean condition is calculated in the catalytic burner keeping the same boundary condition. The inclusion of NO_x kinetics into gas phase kinetics did not affect the concentration of other species or temperatures. To justify the NO_x model, experimental data of Anderson et al. [49] is used for comparison. Though the experiment was done at very high inflow velocity (15–18 m/s) and high pressure (3.8 and 5.2 atm) in a cylindrical burner (0.103 in diameter and 0.31 m long), the NO_x results reported were only dependent on the high flame temperature and fuel compositions. Therefore, NO_x values at a reasonable operating condition in the present catalytic burner are compared. Over the equivalence ratios considered in Fig. 15(a), the NO_x model shows a good agreement with the experiment. The contribution of NO_2 in total emission is computed less than 0.5% in all cases. Thermal NO in Fig. 15(b) is evaluated at the post-processing stage at the same operating condition without considering radiation. The thermal NO obtained 5×10^{-5} ppmv and 0.041 ppmv for $\varphi = 0.25$ (T_{adb} = 1327 K) and $\varphi = 0.39$ (T_{adb} = 1658 K), respectively. Again, the total calculated NO_x for $\varphi = 0.25$ and $\varphi = 0.39$ are 0.09 ppmv and 0.57 ppmv, respectively. By comparison, thermal NO contribution is much less. However, NO_x emission at very lean condition within the range of $0.10 \leq \varphi \leq 0.20$ are computed for two Reynolds numbers of 762 and 1333 as shown in Fig. 16. The NO_x values at Re = 762 for φ = 0.10, 0.13, 0.15, 0.18 and 0.20 are 9.88×10^{-10} ppmv, 2.53×10^{-4} ppmv, 2.58×10^{-3} ppmv, 0.007 ppmv, and 0.016 ppmv, respectively. For Re = 1333, the NOx values have no significant variation for $0.10 \leq \varphi \leq 0.15$ but differ by approximately 0.002 ppmv for φ = 0.18 and 0.20. Furthermore, the NO_x values are comparatively less if radiation loss is considered.

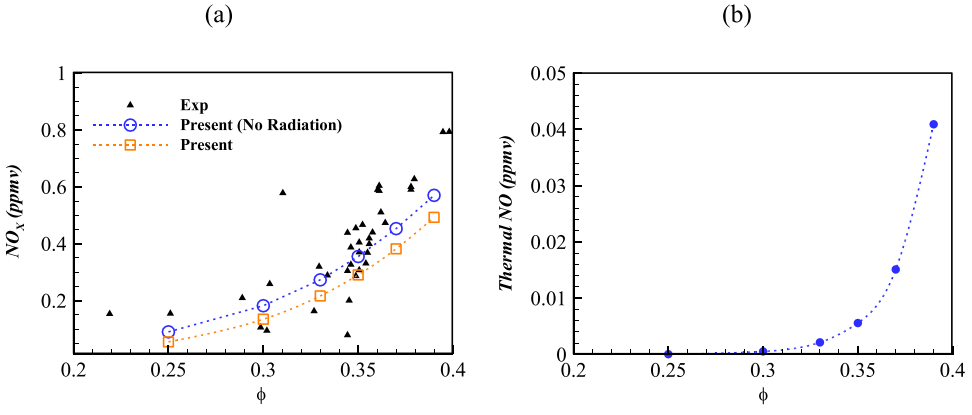

Fig. 15 – Emission as a function of φ using coupled chemistry (CC) (a) NO_x (b) Thermal NO, Re = 1333, T_{in} = 600 K.

Conclusions

Hydrogen/air combustion in a planar burner with platinum coating along its length was numerically investigated. Computations were carried out in multicomponent species transport model of laminar solver using Ansys Fluent. Prior to analysis, the model was validated with available experimental results. To reduce NO_x emission, hydrogen/air lean conditions of equivalence ratio from 0.10 to 0.20 were considered for computation. The key findings of this work are.

- Homogeneous combustion over the range of equivalence ratios from 0.15 to 0.20 in the non-catalytic burner results in an incomplete combustion causing the flame temperature less than the adiabatic temperature. Flame extinction occurs below $Re < 381$ and $Re < 571$ for $\varphi = 0.20$ and 0.18, respectively. No flame is observed for $\varphi \leq 0.16$ over the Re considered.
- In the catalytic configuration, almost complete H_2 conversion is obtained for $0.1 \leq \varphi \leq 0.20$ and both combustion modes (PC/CC) are influenced by the inflow Reynolds number (Re). With φ, the onset of flame ignition shifts toward the inlet.
- The radiation loss at the burner inlet has a significant effect on lowering the flame temperature, which also affects the combustion kinetics.
- Under the wall thermal condition analysed, sufficient catalytic burner length required for complete combustion is influenced by the inflow Reynolds number and residence time.
- NO_x emissions were controlled by N_2O and NNH routes compared to thermal NO. The NO_x values in the catalytic burner increases with φ and can be considered independent on the Reynolds number.

Future study on the planar model will attempt to optimise the catalyst length for cost-effective and NO_x-free operation.

Declaration of competing interest

The authors declare that they have no known competing financial interests or personal relationships that could have appeared to influence the work reported in this paper.

Acknowledgement

The first author greatly acknowledges the receipt of Commonwealth Scholarship award (CSC ID: BDCS-2020-54) and a research grant from Commonwealth Scholarship Commission in the United Kingdom (CSC).

REFERENCES

[1] Mantzaras J. Progress in non-intrusive laser-based measurements of gas-phase thermoscalars and supporting modeling near catalytic interfaces. Prog Energy Combust Sci 2019;70:169–211. https://doi.org/10.1016/j.pecs.2018.10.005.

[2] Bolaños-Chaverri F, Mantzaras J, Griffin T, Bombach R, Winkler D. An experimental and numerical investigation of the catalytic-rich/gaseous-lean combustion of H2/CO/air mixtures at 8 bar. Proc Combust Inst 2021;38:5443–51. https://doi.org/10.1016/j.proci.2020.06.149.

[3] Fumey B, Buetler T, Vogt UF. Ultra-low NOx emissions from catalytic hydrogen combustion. Appl Energy 2018;213:334–42. https://doi.org/10.1016/j.apenergy.2018.01.042.

[4] K W, Lee YSJ. Burner using high-temperature combustion catalyst. Patent No 2021;11. 015,802.

[5] Mantzaras J. Catalytic combustion of hydrogen, challenges, and opportunities. Adv Chem Eng 2014;45:97–157. https://doi.org/10.1016/B978-0-12-800422-7.00003-0. Academic Press Inc.

[6] Piemsinlapakunchon T, Paul MC. Effect of syngas fuel compositions on the occurrence of instability of laminar diffusion flame. Int J Hydrogen Energy 2021;46:7573–88. https://doi.org/10.1016/j.ijhydene.2020.11.259.

[7] du Toit MH, Avdeenkov Av, Bessarabov D. Reviewing H_2 combustion: a case study for non-fuel-cell power systems and safety in passive autocatalytic recombiners. Energy Fuel 2018;32:6401–22. https://doi.org/10.1021/acs.energyfuels.8b00724.

[8] Nguyen VN, Deja R, Peters R, Blum L, Stolten D. Study of the catalytic combustion of lean hydrogen-air mixtures in a monolith reactor. Int J Hydrogen Energy 2018;43:17520–30. https://doi.org/10.1016/j.ijhydene.2018.07.126.

[9] Pizza G, Frouzakis CE, Mantzaras J, Tomboulides AG, Boulouchos K. Dynamics of premixed hydrogen/air flames in mesoscale channels. Combust Flame 2008;155:2–20. https://doi.org/10.1016/j.combustflame.2008.08.006.

[10] Pizza G, Frouzakis CE, Mantzaras J. Chaotic dynamics in premixed hydrogen/air channel flow combustion. Combust Theor Model 2012;16:275–99. https://doi.org/10.1080/13647830.2011.620174.

[11] Pizza G, Frouzakis CE, Mantzaras J, Tomboulides AG, Boulouchos K. Dynamics of premixed hydrogen/air flames in microchannels. Combust Flame 2008;152:433–50. https://doi.org/10.1016/j.combustflame.2007.07.013.

[12] Schefer R. Evaluation of NASA lean premixed hydrogen burner, Albuquerque, NM, and Livermore, CA (United States). 2003. https://doi.org/10.2172/811192.

[13] Yang W, Deng C, Zhou J, Liu J, Wang Y, Cen K. Experimental and numerical investigations of hydrogen-air premixed combustion in a converging-diverging micro tube. Int J Hydrogen Energy 2014;39:3469–76. https://doi.org/10.1016/j.ijhydene.2013.12.102.

[14] Pers H, Aniello A, Morisseau F, Schuller T. Autoignition-induced flashback in hydrogen-enriched laminar premixed burners. Int J Hydrogen Energy 2022. https://doi.org/10.1016/j.ijhydene.2022.12.041.

[15] Yan Y, Zhang C, Gao J, Shen K, Gao W. Numerical study on premixed hydrogen/air combustion characteristics and heat transfer enhancement of micro-combustor embedded with pin fins. Int J Hydrogen Energy 2021;46:38519–34. https://doi.org/10.1016/j.ijhydene.2021.09.097.

[16] Wu S, Abubakar S, Li Y. Thermal performance improvement of premixed hydrogen/air fueled cylindrical micro-combustor using a preheater-conductor plate. Int J Hydrogen Energy 2021;46:4496–506. https://doi.org/10.1016/j.ijhydene.2020.10.237.

[17] Fernández A, Arzac GM, Vogt UF, Hosoglu F, Borgschulte A, Jiménez de Haro MC, Montes O, Züttel A. Investigation of a Pt containing washcoat on SiC foam for hydrogen combustion applications. Appl Catal, B 2016;180:336–43. https://doi.org/10.1016/j.apcatb.2015.06.040.

[18] Ghermay Y, Mantzaras J, Bombach R, Boulouchos K. Homogeneous combustion of fuel-lean H2/O2/N2 mixtures over platinum at elevated pressures and preheats. Combust Flame 2011;158:1491–506. https://doi.org/10.1016/j.combustflame.2010.12.025.
[19] Schlegel A. Catalytic stabilization of lean premixed combustion: method for improving NOx emissions. Combust Flame 1996;105:332–40. https://doi.org/10.1016/0010-2180(95)00211-1.
[20] Vlachos DG. Homogeneous-heterogeneous oxidation reactions over platinum and inert surfaces. Chem Eng Sci 1996;51:2429–38. https://doi.org/10.1016/0009-2509(96)00099-1.
[21] Appel C, Mantzaras J, Schaeren R, Bombach R, Inauen A, Kaeppeli B, Hemmerling B, Stampanoni A. An experimental and numerical investigation of homogeneous ignition in catalytically stabilized combustion of hydrogen/air mixtures over platinum. Combust Flame 2002;128:340–68.
[22] Pizza G, Mantzaras J, Frouzakis CE, Tomboulides AG, Boulouchos K. Suppression of combustion instabilities of premixed hydrogen/air flames in microchannels using heterogeneous reactions. Proc Combust Inst 2009;32:3051–8. https://doi.org/10.1016/j.proci.2008.05.055.
[23] Choi W, Kwon S, Dong Shin H. Combustion characteristics of hydrogen-air premixed gas in a sub-millimeter scale catalytic combustor. Int J Hydrogen Energy 2008;33:2400–8. https://doi.org/10.1016/j.ijhydene.2008.02.070.
[24] Zhang Y, Pan J, Lu Z, Tang A, Zhu Y, Bani S. The characteristics of pure heterogeneous reaction for H2/Air mixture in the micro-combustors with different thermophysical properties. Appl Therm Eng 2018;141:741–50. https://doi.org/10.1016/j.applthermaleng.2018.06.021.
[25] Zhang Y, Pan J, Lu Q, Wang Y, Li J, Quaye EK, Weng J. Numerical investigation on the self-ignition and combustion characteristics of H2/air in catalytic micro channel. Int J Hydrogen Energy 2022;47:1965–78. https://doi.org/10.1016/j.ijhydene.2021.10.112.
[26] Sui R, Mantzaras J. Combustion stability and hetero-/homogeneous chemistry interactions for fuel-lean hydrogen/air mixtures in platinum-coated microchannels. Combust Flame 2016;173:370–86. https://doi.org/10.1016/j.combustflame.2016.08.011.
[27] Mantzaras J, Bombach R, Schaeren R. Hetero-/homogeneous combustion of hydrogen/air mixtures over platinum at pressures up to 10bar. Proc Combust Inst 2009;32:1937–45. https://doi.org/10.1016/j.proci.2008.06.067.
[28] Lu Q, Gou J, Wang Y, Fan B, Zhang Y, Wang Y, Quaye EK, Pan J. Thermal and chemical analysis on the hetero-/homogeneous combustion characteristics of H2/Air mixture in a micro channel with catalyst segmentation. Fuel 2022;320:123883. https://doi.org/10.1016/j.fuel.2022.123883.
[29] Tang A, Xu Y, Shan C, Pan J, Liu Y. A comparative study on combustion characteristics of methane, propane and hydrogen fuels in a micro-combustor. Int J Hydrogen Energy 2015;40:16587–96. https://doi.org/10.1016/j.ijhydene.2015.09.101.
[30] Chen J, Yan L, Song W. Effect of the gas-phase reaction on hydrogen microcombustion in a Pt/γ-Al2O3 catalytic plane channel with detailed chemical kinetic mechanisms. Prog React Kinet Mech 2015;40:1–21. https://doi.org/10.3184/146867815X14212355041114.
[31] Sui R, Prasianakis NI, Mantzaras J, Mallya N, Theile J, Lagrange D, Friess M. An experimental and numerical investigation of the combustion and heat transfer characteristics of hydrogen-fueled catalytic microreactors. Chem Eng Sci 2016;141:214–30. https://doi.org/10.1016/j.ces.2015.10.034.
[32] Lu Q, Pan J, Yang W, Pan Z, Tang A, Zhang Y. Effects of products from heterogeneous reactions on homogeneous combustion for H2/O2 mixture in the micro combustor. Appl Therm Eng 2016;102:897–903. https://doi.org/10.1016/j.applthermaleng.2016.04.052.
[33] Lu Q, Gou J, Pan J, Zhang Y, Zhu J, Quaye EK. Comparison of the effect of heat release and products from heterogeneous reaction on homogeneous combustion of H2/O2 mixture in the catalytic micro combustor. Int J Hydrogen Energy 2019;44:31557–66. https://doi.org/10.1016/j.ijhydene.2019.10.040.
[34] Zhang Y, Pan J, Tang A, Liu Y, Pan Z, Lu Q, Otchere P. Effect of gas-phase reaction on catalytic reaction for H2/O2 mixture in micro combustor. Int J Hydrogen Energy 2017;42:16855–65. https://doi.org/10.1016/j.ijhydene.2017.05.117.
[35] Pan J, Miao N, Lu Z, Lu Q, Yang W, Pan Z, Zhang Y. Experimental and numerical study on the transition conditions and influencing factors of hetero-/homogeneous reaction for H2/Air mixture in micro catalytic combustor. Appl Therm Eng 2019;154:120–30. https://doi.org/10.1016/j.applthermaleng.2019.03.076.
[36] Merk HJ. The macroscopic equations for simultaneous heat and mass transfer in isotropic, continuous and closed systems. Appl Sci Res 1959;8:73–99. https://doi.org/10.1007/BF00411741.
[37] Deutschmann O, Schmidt R, Behrendt F, Warnat J. Numerical modeling of catalytic ignition. In: Symposium (International) on Combustion. 26; 1996. p. 1747–54. https://doi.org/10.1016/S0082-0784(96)80400-0.
[38] Warnatz J, Allendorf MD, Kee RJ, Coltrin ME. A model of elementary chemistry and fluid mechanics in the combustion of hydrogen on platinum surfaces. Combust Flame 1994;96:393–406. https://doi.org/10.1016/0010-2180(94)90107-4.
[39] Kee R, Rupley F, Miller J. Chemkin-II: a Fortran chemical kinetics package for the analysis of gas-phase chemical kinetics. Albuquerque, NM, and Livermore, CA (United States). 1989. https://doi.org/10.2172/5681118.
[40] Coltrin ME, Kee RJ, Rupley FM, Meeks E. Surface CHEMKIN-III: a Fortran package for analyzing heterogeneous chemical kinetics at a solid-surface - gas-phase interface, Albuquerque, NM, and Livermore, CA (United States). 1996. https://doi.org/10.2172/481906.
[41] R.J.D.-L.G.W.J.C.M.E., Kee MJA. A Fortran computer code package for the evaluation of gas-phase, multicomponent transport properties. 1986. United States.
[42] Zeldovich J. The oxidation of nitrogen in combustion and explosions. Eur Phys J Hadr Nuclei 1946;21:577–628. ISSN: 1434-6001 EISSN: 1434-601X.
[43] Glarborg P, Miller JA, Ruscic B, Klippenstein SJ. Modeling nitrogen chemistry in combustion. Prog Energy Combust Sci 2018;67:31–68. https://doi.org/10.1016/j.pecs.2018.01.002.
[44] Howard Carleton J. Kinetic study of the equilibrium HO2+ NO. dblarw. OH+ NO2 and the thermochemistry of HO2. J Am Chem Soc 1980;102:6937–41.
[45] Deutschmann O, Maier LI, Riedel U, Stroemman AH, Dibble RW. Hydrogen assisted catalytic combustion of methane on platinum. Catal Today 2000;59:141–50. https://doi.org/10.1016/S0920-5861(00)00279-0.
[46] Ghermay Y, Mantzaras J, Bombach R. Effects of hydrogen preconversion on the homogeneous ignition of fuel-lean H2/O2/N2/CO2 mixtures over platinum at moderate pressures. Combust Flame 2010;157:1942–58. https://doi.org/10.1016/j.combustflame.2010.02.016.
[47] Schultze M, Mantzaras J. Hetero-/homogeneous combustion of hydrogen/air mixtures over platinum: fuel-lean versus

fuel-rich combustion modes. Int J Hydrogen Energy 2013; 38:10654–70. https://doi.org/10.1016/j.ijhydene.2013.06.069.
[48] Weiland WF. Measurement of local heat transfer coefficients for flow of hydrogen and helium in a smooth tube at high surface to fluid bulk temperature ratios. In: Symposium on nuclear engineering heat transfer, Chicago, Illinois; 1962.
[49] Anderson David N. Emissions of oxides of nitrogen from an experimental premixed -hydrogen burner. Ohio 1976;44135.